

Photovoltaic reverse osmosis — Feasibility and a pathway to develop technology

Amy M. Bilton^{a*}, Leah C. Kelley^b, Steven Dubowsky^b

^aDepartment of Aeronautics and Astronautics, ^bDepartment of Mechanical Engineering,
Massachusetts Institute of Technology, Cambridge, MA 02139, USA
Tel. +1 (617) 253-5095; Fax +1 (617) 258-7881; email: bilton@mit.edu

Received 13 October 2010; Accepted in revised form 7 December 2010

ABSTRACT

Small-scale photovoltaic-powered reverse osmosis (PVRO) desalination plants can provide fresh water to remote communities that do not have sufficient natural sources. For these systems to be practical, they must be both technically and economically feasible. This paper presents a research program that is focused on improving the feasibility of PVRO systems. As the first step in this program, a methodology to evaluate the economic feasibility was developed. The results, reviewed here, show that the economic feasibility is a strong function of location. The results also show that increasing the efficiency of PVRO systems can extend their feasibility to currently marginal or unfeasible locations. A focus of this research program is the development of smart control algorithms to increase system efficiency and improve feasibility. This paper presents PVRO system models which have been developed to evaluate the smart control algorithms. These models are verified using an experimental system also described here. Early experimental results are presented that show good agreement with the analytical models.

Keywords: Photovoltaic; Reverse osmosis; Feasibility; Remote communities

1. Introduction

1.1. Motivation

Approximately 1.2 billion people worldwide do not have access to adequate clean water [1]. Many of these people live in small remote communities off of the main water grid. That number will increase with population growth and global warming [2,3]. Alternative water solutions are required for these locations.

Remote communities are often located in areas with access to seawater or brackish groundwater. For such

communities, small-scale reverse osmosis (RO) desalination can provide fresh water. Desalination is an energy intensive process. Diesel generators or grid power are commonly used to power RO systems; however, diesel generators pollute the environment and their fuel is expensive. Grid power may not be available or may be expensive. Using photovoltaics to power RO desalination systems is a promising solution for such communities.

Here, the economic feasibility of photovoltaic reverse osmosis (PVRO) systems is briefly reviewed. From these results it is clear that a key to extending the utility of PVRO is improving its efficiency. This paper then presents our research program's pathway to meet this objective.

* Corresponding author.

1.2. Background and literature review

There are well-established desalination technologies to produce water for large communities, such as reverse osmosis and thermal desalination. Thermal processes work well for large communities, but they do not scale well for smaller communities. Reverse osmosis desalination systems can be scaled more easily for the demands of smaller communities.

PVRO systems have been proposed [4–8]. Early systems simply combined a photovoltaic array and batteries to power an existing reverse osmosis desalination system. Battery-based systems were found to be inefficient and expensive. Recent research has focused on increasing system efficiency with some success [4,5]. Photovoltaic-powered reverse osmosis systems without batteries have also been the subject of significant research [6,7].

These studies show that PVRO systems are technically feasible. However, for PVRO to be practical, it must be economically competitive with alternative, conventional methods. In this research program, the economic feasibility of PVRO systems for small communities has been studied [9]. The results of this study, summarized in Section 2, show the current efficiency of these systems limit the use of PVRO for many communities.

1.3. Overview of the research program

Increasing overall PVRO system efficiency can potentially increase the locations where PVRO systems are practical. Substantial research is being done to improve the efficiency of individual system components, such as solar cells and reverse osmosis membranes; however, little research is currently being done on optimizing the overall system performance using system control methods.

One of the major challenges associated with the control of small-scale PVRO systems is accommodating variations in the solar radiation. This variation requires the system to adjust its settings to maintain its maximum water production. Variations in other system factors, such as air temperature, water temperature, and water source salinity, also require adjustments to the system. The common solution for dealing with variations in solar radiation is to include batteries to store energy; however, batteries are expensive and have limited lives. The approach taken here will consider system configurations without batteries. The system operation must be adjusted continuously to maximize water output while maintaining water quality and prolonging system component lives. Autonomous control is also required, since it is not practical for an operator to monitor a small-scale PVRO system continuously.

To achieve these objectives, a series of PVRO system models, described below, have been developed to evaluate system and control algorithm performance. A small-scale experimental system has been designed and fabricated to validate the system models and evaluate

control approaches. Details of the system design and sample experimental data are presented. The system models show good agreement with preliminary experimental results.

2. Feasibility study

A feasibility study was conducted as a first step in this research program [9]. As discussed above, PVRO systems have been developed and shown to be technically feasible. To be practical, however, these systems must also be economically feasible. Economic feasibility studies of PVRO systems have been conducted in the past for specific locations, such as Oman, Greece and the United Arab Emirates [10–12]. Studies of these results show that feasibility of PVRO systems is critically dependent on location. A generalized method to determine economic feasibility as a function of location had not yet been done.

In our feasibility study, a generalized method to evaluate the economic feasibility of small-scale PVRO systems as a function of location is developed. The economic feasibility is determined by comparing the PVRO water cost with that of water provided by conventional methods. The common methods to provide fresh water to remote, water scarce regions is by transporting water or by using diesel powered water desalination. Feasible regions are those where the cost of water produced by the PVRO system is less than the cost of transported water, and the total system lifetime cost of the PVRO system is less expensive than an equivalent diesel-powered reverse osmosis system.

To determine economic feasibility, the full lifecycle costs of both the photovoltaic-powered and diesel-powered reverse osmosis systems were calculated. The lifecycle costs were broken into two components: the system capital costs and operating costs. These costs are determined for a location based on the local solar resource, water characteristics and water demands.

A simple schematic of the PVRO system considered is shown in Fig. 1. (The difference between the PVRO and diesel generator system is the power source; otherwise a schematic for the diesel system is identical.) Here, the energy source powers a feed pump and a high-pressure pump to pressurize the incoming water. The high pressure produced by the pumps drive the water through the reverse osmosis membrane, leaving high pressure brine that passes through a turbine to recover its energy before exiting the system.

An energy analysis was performed to determine the reverse osmosis system capacity, solar array size, diesel generator size and diesel fuel consumption rate for a given water production and location. Since it was assumed that the photovoltaic-powered system does not have batteries, it only runs during the daytime. The diesel-powered system is assumed to run 24 h/d. Local political factors, such as incentives and carbon taxes are not included. The

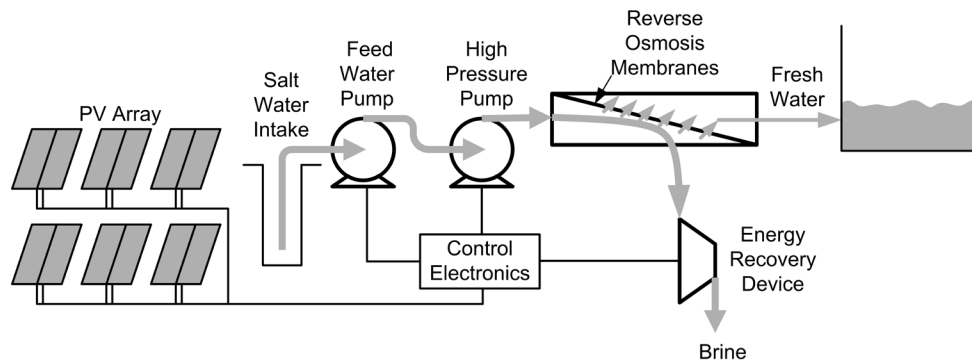


Fig. 1. Simple photovoltaic reverse osmosis system considered in evaluation.

cost of water produced by the diesel-powered and PVRO systems was then determined using the equivalent annualized cost method [13]. The PVRO system is considered economically feasible if the calculated water cost is less than the cost of water produced by the diesel-powered system and that of transported water [9].

Geographic Information Systems (GIS) data of annual solar insolation [14] and water characteristics [15] are used in the analysis. Cost data, component lifetimes and maintenance schedules are taken from the published literature. The key parameters for the cost analysis are shown in Table 1 [9].

The overall water cost for the PVRO systems is shown in Fig. 2. The majority of the equatorial regions are able to produce water for less than \$6.00/m³. PVRO systems are able to produce water at a cost of less than \$5.00/m³ in many water-stressed areas, such as the Middle East.

The regions where the PVRO system is more cost effective than the diesel-powered system are shown in Fig. 3, and include large areas of water scarce regions. The coastal regions of northern Africa, the Middle East, South Africa, Mexico and the Caribbean are all examples of water stressed areas where a seawater PVRO system could feasibly deliver clean water to small communities at a lower cost than diesel-powered reverse osmosis systems.

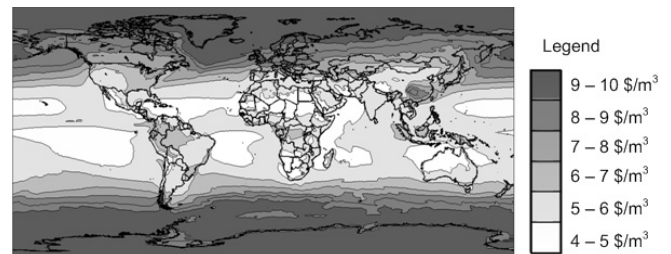


Fig. 2. Cost of water (\$/m³) for solar powered system [9].

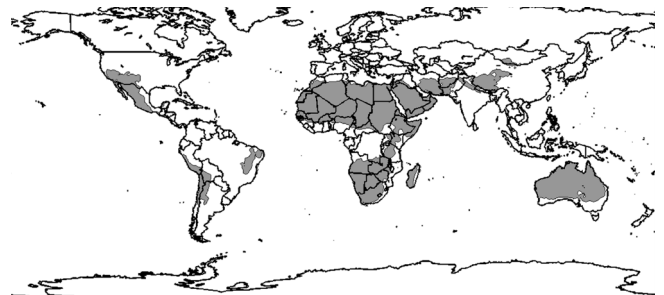


Fig. 3. Areas where a solar powered system is less expensive than a diesel system without government incentives [9].

Table 1
Input parameters for seawater reverse osmosis analysis [9]

Parameter	Value
Plant capacity	10 m ³
Plant lifetime	25 years
Interest rate	5%
Plant capacity factor	90%
Recovery ratio	40%
Reverse osmosis system cost [13]	\$2400/m ³
Installed array system cost [16]	\$9.00/Wp
Initial diesel fuel cost [17]	\$0.66/L (\$2.50/gallon)

Table 2 shows the details for six representative locations. As expected, the areas with higher water salinity require more energy to perform reverse osmosis, and the areas listed with the low solar insolation are not favorable for the solar powered systems. For the price assumptions made, the PVRO system is less expensive than the diesel system for all of the sites except Boston and Los Angeles. In general, PVRO is feasible in areas with a high solar resource.

The results of the study show the clear location dependency of PVRO feasibility. This dependency is due to the differences in water demand, water characteristics and solar resources. They also show that the PVRO is feasible

Table 2
Site specific analysis results — seawater reverse osmosis without incentives and carbon tax [9]

Location	Boston, USA	Los Angeles, USA	Limissol, Cyprus	Aqaba, Jordan	Cap-Haïtien, Haiti	Jeddah, Saudi Arabia
Latitude	42.35 N	34.05 N	34.67 N	29.52 N	19.76 N	16.89 N
Longitude	71.06 W	118.24 W	33.03 E	35.07 E	72.2 W	42.55 E
Average latitude tilt solar insolation (kWh/m ² -d)	4.4	5.6	6.1	5.9	6.1	6.6
Daylight hours (h)	9.08	9.88	9.87	10.25	10.93	11.13
Water salinity (ppm)	32664	33505	39182	41160	36275	38340
Energy required per day (kWh)	29.2	30.1	34.1	35.7	31.9	33.4
Solar array area (m ²)	44.2	35.8	37.3	40.3	34.8	33.7
Total PVRO system capital cost (\$)	149,830	123,349	120,049	125,696	118,296	111,748
PVRO system equiv. annual cost (\$)	21,757	17,524	16,568	17,265	16,523	15,447
Total diesel system capital cost (\$)	46,718	46,644	46,362	46,279	46,497	46,445
Diesel system equiv. annual cost (\$)	17,147	17,295	17,983	18,231	17,626	17,758
Cost of water solar (\$/m ³)	6.62	5.33	5.04	5.25	5.02	4.70
Cost of water diesel (\$/m ³)	5.21	5.25	5.47	5.54	5.36	5.41

for many water-stressed regions. The high fuel costs for the diesel-powered systems result in higher water costs for most locations. When the system is configured for a region without high solar resource, the high capital costs for community-scale seawater PVRO systems are not recovered during the system lifetime. With intelligent system control of the PVRO systems, it is possible to further reduce system costs, thus the PVRO systems could become affordable for larger regions.

3. System modeling

Full non-linear system models have been developed for PVRO systems. The models incorporate the key factors that affect PVRO system performance, including solar radiation, water salinity, water temperature, air temperature and water demand. A representative PVRO system with stochastic system inputs is shown in Fig. 4.

The PVRO system models have been developed in Matlab/Simulink. A high-level block diagram of a simple PVRO system is shown in Fig. 5. These models were

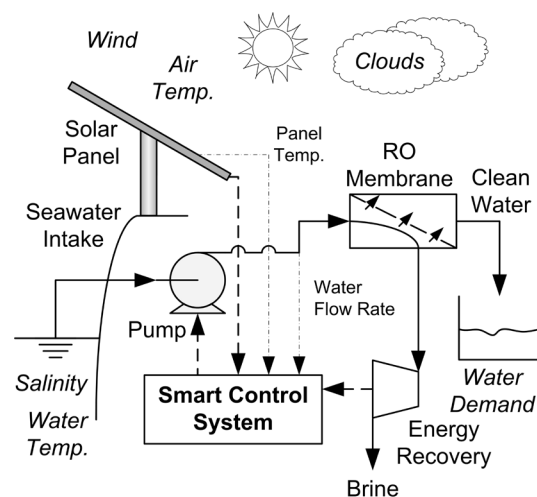


Fig. 4. PVRO system schematic.

constructed at the individual component level, and are a blend of physics-based and empirical equations. Full

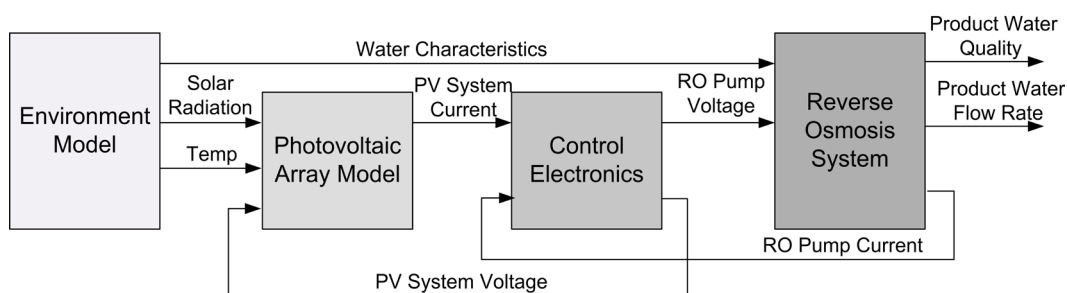


Fig. 5. High-level PVRO system model block diagram.

presentation of all model equations is beyond the scope of this paper. Here, only the key concepts are presented.

3.1. Solar energy model

A simple model was developed to estimate the solar energy available during a clear day. For a given latitude, longitude and time, the solar elevation and azimuth are well-known [18]. This model is used to estimate the direct, diffuse and reflected portions of solar radiation [19]. Then, the amount of direct radiation incident on the panel can be found using the following equation:

$$G_{\text{mod,dir}} = G_{\text{dir}} [\cos \alpha \sin \beta \cos(\psi - \theta) + \sin \alpha \cos \beta] \quad (1)$$

where G_{dir} is the direct insolation on a plane normal to the incoming sun rays, α is the sun elevation angle, β is the module tilt angle, ψ is the module azimuth angle, and θ is the azimuth angle of the sun. The total insolation incident on the panel surface is given by:

$$G_{\text{mod,dir}} = G_{\text{mod,dir}} + G_{\text{mod,dif}} + G_{\text{mod,ref}} \quad (2)$$

where $G_{\text{mod,dif}}$ and $G_{\text{mod,ref}}$ are the diffuse and reflected radiation received by the panel, respectively.

3.2. Solar array model

For the PV panel, each individual solar cell is represented using the classic two-diode model, given by [20]:

$$I_{\text{cell}} = I_{\text{ph}} - I_{D1} - I_{D2} - \frac{V + I_{\text{cell}} R_s}{R_{\text{sh}}} \quad (3)$$

where I_{cell} is the cell current, I_{ph} represents the light generated current, I_{D1} and I_{D2} represent the losses due to recombination (which are temperature dependent), V is the solar cell operating voltage, R_s is the solar cell series resistance in ohms, and R_{sh} is the solar cell shunt resistance in ohms. The light-generated current is given by:

$$I_{\text{ph}} = A_c (C_0 + C_1 T_{\text{cell}}) G_{\text{mod,tot}} \quad (4)$$

where A_c is the solar cell area in m^2 , C_0 and C_1 are solar cell-specific constants, T_{cell} is the cell temperature in Kelvin, and $G_{\text{mod,tot}}$ is the incoming solar radiation in W/m^2 .

The cell temperature at a given solar radiation is given by the following empirical relationship:

$$T_{\text{cell}} = T_{\text{amb}} + \frac{G_{\text{mod,tot}} (\text{NOCT} - 293.15)}{800} \quad (5)$$

where T_{amb} is the ambient temperature in Kelvin, NOCT is the normal operating cell temperature in Kelvin, and $G_{\text{mod,tot}}$ is the total incident solar insolation on the module in W/m^2 .

The solar panel model was developed by connecting the individual solar cell models into strings in series, and then connecting the strings in parallel. In this model, all cells are assumed identical. For the series connections,

the current through all of the cells is the same and the voltage adds, so Eq. (3) applies. Voltage V_{string} and current I_{string} for cells connected in a series string are found using:

$$V_{\text{string}} = n_{\text{cell}} V_{\text{cell}} \quad (6)$$

$$I_{\text{string}} = I_{\text{cell}} \quad (7)$$

where n_{cell} is the number of cells connected in the string.

For the parallel string connections, the voltage remains the same and the currents add. This relationship is expressed as follows:

$$I_{\text{module}} = n_{\text{string}} I_{\text{string}} \quad (8)$$

$$V_{\text{module}} = V_{\text{string}} \quad (9)$$

where I_{module} is the current of the module, V_{module} is the module voltage, and n_{string} is the number of strings connected in parallel.

3.3. Control electronics

The control electronics and computer take the power being produced by the solar array and condition it for use by the reverse osmosis system motors and pumps. In this portion of the model, different control algorithms can be implemented to control the operating point of the PVRO system. Since the systems considered here do not use batteries and the power conversion is not perfect, the following relationship is used:

$$V_{\text{motor}} I_{\text{motor}} = \eta_{\text{mppt}} V_{\text{module}} I_{\text{module}} \quad (10)$$

where V_{motor} is the motor voltage, I_{motor} is the motor current and η_{mppt} is the power conversion efficiency from the solar module to the motor, and V_{module} and I_{module} are the voltage and current of the solar module found from Eqs. (8) and (9).

3.4. Motor

A simple static motor model, with motor resistance assumed constant, was used to estimate the system performance. The shaft torque τ can be expressed using the following equation:

$$\tau = (I_{\text{motor}} - I_0) / K_T \quad (11)$$

where I_{motor} is the motor current, I_0 is the friction related current, and K_T is the torque constant.

The internal back-EMF, V_m is assumed to be proportional to the rotor speed Ω via the motor speed constant K_v as shown:

$$V_m = \Omega / K_v \quad (12)$$

The motor terminal voltage V_{motor} can be found by

adding the resistive voltage drop to the back-EMF, V_m as shown:

$$V_{\text{motor}} = V_m + I_{\text{motor}} R_m = \frac{\Omega}{K_V} + I_{\text{motor}} R_m \quad (13)$$

where R_m is the resistance of the motor in Ohms.

3.5. Pump

Due to the pressures and flow rates involved in the reverse osmosis system, positive displacement pumps are commonly used. The flow rate produced by a positive displacement pump Q is found using:

$$Q = Dn - c_s \frac{D}{2\pi} \frac{\Delta p}{\mu} - Q_R \quad (14)$$

where n is the pump speed in revolutions per minute, D is the pump volumetric displacement per revolution, c_s is the pump slip coefficient, μ is the dynamic viscosity of the water, Δp is the pressure difference across the pump, and Q_R is the flow loss due to inlet flow restriction.

The torque required by a positive displacement pump is given by:

$$\tau = 100 \frac{\Delta p D}{2\pi} + c_d D \mu n + c_f \frac{D}{2\pi} \Delta p + T_c \quad (15)$$

where c_d is the coefficient of viscous drag, c_f is the coefficient of friction for the pump geometry, and T_c is the pump torque constant. Since the motor and pump share the same shaft, the speed and torque of the motor and pump are identical.

3.6. Energy recovery

There are many different types of reverse osmosis energy recovery devices. The presentation of the full set of equations describing the energy recovery is beyond the scope of this paper. For full details, refer to [6].

Here, the Clark Pump pressure exchanger produced by Spectra Watermakers [5] is described. The Clark pump is a fixed-ratio pressure exchanger consisting of two pistons connected with a rod, as shown in Fig. 6. When the piston reaches the end of travel, a reversing valve switches the brine and exhaust connections, and the piston reverses direction. The area of the rod changes the effective areas on either side of the piston, and the device adds the energy in the medium pressure feed to the energy in the concentrate, producing water at a higher pressure than the concentrate.

The recovery ratio, R_r of a reverse osmosis system using the Clark pump is defined as [6]:

$$R_r = \frac{A_r}{A_p} = \frac{Q_p}{Q_f} \quad (16)$$

where A_p is the area of the piston, A_r is the area of the

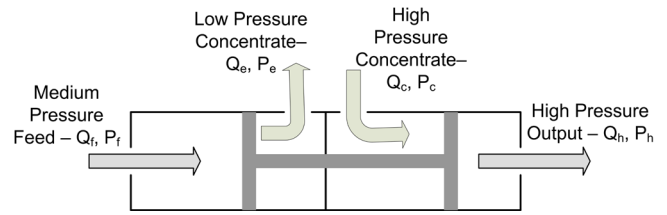


Fig. 6. Basic Clark pump mechanics.

connecting rod, Q_p is the fresh water flow rate, and Q_f is the medium pressure feed flow rate. Using the recovery ratio, the relationships for the fresh water flow rate Q_p and brine flow rate Q_e , respectively, are [6]:

$$Q_p = R_r Q_f - Q_L \quad (17)$$

$$Q_e = Q_f (1 - R_r) + Q_L \quad (18)$$

where Q_L are the leakage flow rates in the Clark pump, found empirically using [6]:

$$Q_L = 1.78 \times 10^{-4} Q_f P_H + 1.56 \times 10^{-5} \quad (19)$$

where P_H is the pressure of the feed water entering the RO pressure vessel.

The feed water pressure is found by balancing the forces on the piston, and can be defined in terms of the recovery ratio as [6]:

$$P_H = P_f + P_c (1 - R_r) - (1 - R_r) - P_L \quad (20)$$

where P_f is the pressure of the feed water entering the Clark pump, P_c is the pressure of the brine entering the pump, P_e is the pressure of the brine exiting the pump, and P_L are the pressure losses in the pump. The pressure losses are defined empirically using [6]:

$$P_L = 49.2 Q_f^2 + 7.09 \times 10^{-2} \Delta P + 0.528 \quad (21)$$

where Q_f is the feed flow rate in L/s and $\Delta P = P_H - P_c$ in bar.

3.7. Reverse osmosis membrane

An RO membrane is a cross-flow separator. The flow of fresh water out of the membrane can be written as:

$$Q_p = A S_E (\text{TCF})(\text{FF}) (\Delta \bar{P} - \Delta \bar{\pi}) \quad (22)$$

where S_E is the membrane surface area, A is the membrane permeability for water, TCF is the water permeability temperature correction factor, FF is the membrane fouling factor, $\Delta \bar{P}$ is the average pressure applied across the membrane, and $\Delta \bar{\pi}$ is the average osmotic pressure applied across the membrane. Here, empirical relations from Dow [21] are used to determine the temperature correction factor, and the fouling factor is not currently

estimated.

The average pressure applied across the membrane is found using:

$$\Delta \bar{P} = P_H - \frac{\Delta P_{fc}}{2} - P_p \quad (23)$$

where P_p is the pressure of the fresh water exiting the membrane and ΔP_{fc} is the pressure drop over the membrane module, estimated empirically using [21]:

$$\Delta P_{fc} = 0.756 \left(\frac{Q_C + Q_F}{2} \right)^{1.7} \quad (24)$$

where Q_C and Q_F are the brine and feed flow rates in L/s, respectively. The pressure drop over the membrane can also be used to calculate the pressure in the exiting brine using:

$$P_C = P_H - \Delta P_{fc} \quad (25)$$

The average difference in osmotic pressure is calculated using:

$$\Delta \bar{\pi} = (pf) \frac{\pi_f + \pi_b}{2} - \pi_p \quad (26)$$

where pf is the concentration polarization factor, π_f is the osmotic pressure of the feed, π_b is the osmotic pressure of the brine, and π_p is the osmotic pressure of the fresh water. The osmotic pressure is estimated using an empirical relationship from the ASTM Standards [22], and the polarization factor is estimated using an empirical relationship derived by Dow [21].

Since separation across an RO membrane is not perfect, some salt is also transmitted across the membrane in the fresh water. The concentration of salt in the fresh water is given by:

$$C_p = \frac{BS_E (pf)(TCF)C_{cf}}{Q_p} \quad (27)$$

where B is the membrane permeability to salt and C_{fc} is the average concentration of the water on the concentrate side of the membrane, given by:

$$C_{fc} = \frac{C_f + C_b}{2} \quad (28)$$

where C_f is the salt concentration in the feed water and C_b is the salt concentration in the exiting brine. Finally, since salt water flow is considered incompressible, the flow of both water and salt are conserved:

$$Q_F = Q_C + Q_p \quad (29)$$

$$Q_F C_f = Q_C C_b + Q_p C_p \quad (30)$$

Eqs. (1)–(30) are a complex set of nonlinear quasi-static equations whose solution has been implemented in Matlab/Simulink using the structure shown in Fig. 5.

The ode45 solver is used to simultaneously solve the system of equations. This complete model forms the core of our optimal control algorithm development. To ensure that these models are sound, they are validated with our experimental system, described below.

4. Experimental system

The MIT system has been constructed on a campus rooftop (see Fig. 7). This system is modular and reconfigurable. It is composed of a tracking PV panel, custom control electronics, parallel DC pumps, a Clark pump energy recovery system, reverse osmosis membrane within a pressure vessel, and plastic water tanks. The system does not use batteries for power leveling. Small batteries are used as backup power for the electronics. The system is fully instrumented and computer controlled to optimize the system water output, and is designed to produce approximately 300 L of fresh water per day in Boston on a sunny summer day.

The system instrumentation consists of 18 different sensors that provide sufficient information for model validation and control feedback (see Fig. 8). Sensors include thermistors for measuring solar panel, feed water, and ambient air temperature, flow sensors, salinity sensors, pressure transducers, and sensors for measuring solar panel orientation. The sensors are connected via custom electronics to the data acquisition and control computer, shown in Fig. 9.

Two PIC24 microcontrollers in a Master/Slave configuration are used to acquire sensor data through a sensor conditioning board, and to perform computation and control tasks. The Master PIC24 is used to control a DC/DC step down converter that receives power from the solar panels and converts it to the voltage desired by the two DC boost pumps. The Slave PIC24 is used to drive

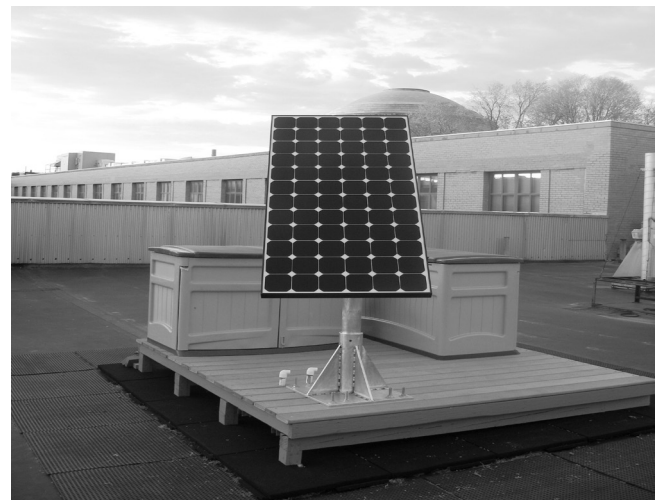


Fig. 7. Experimental system setup.

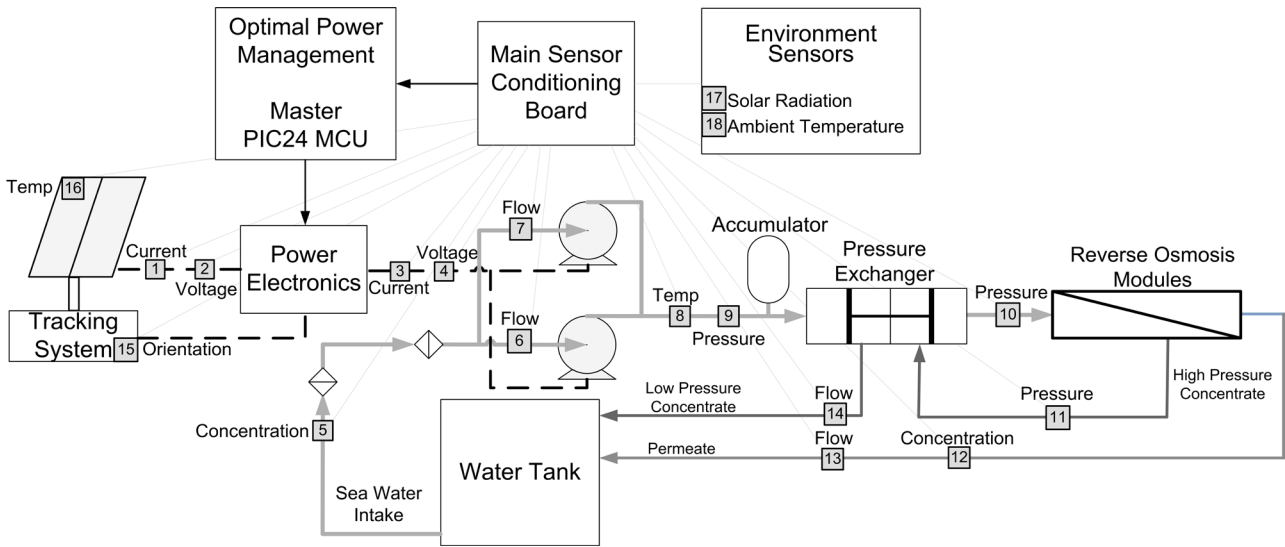


Fig. 8. Experimental system layout.

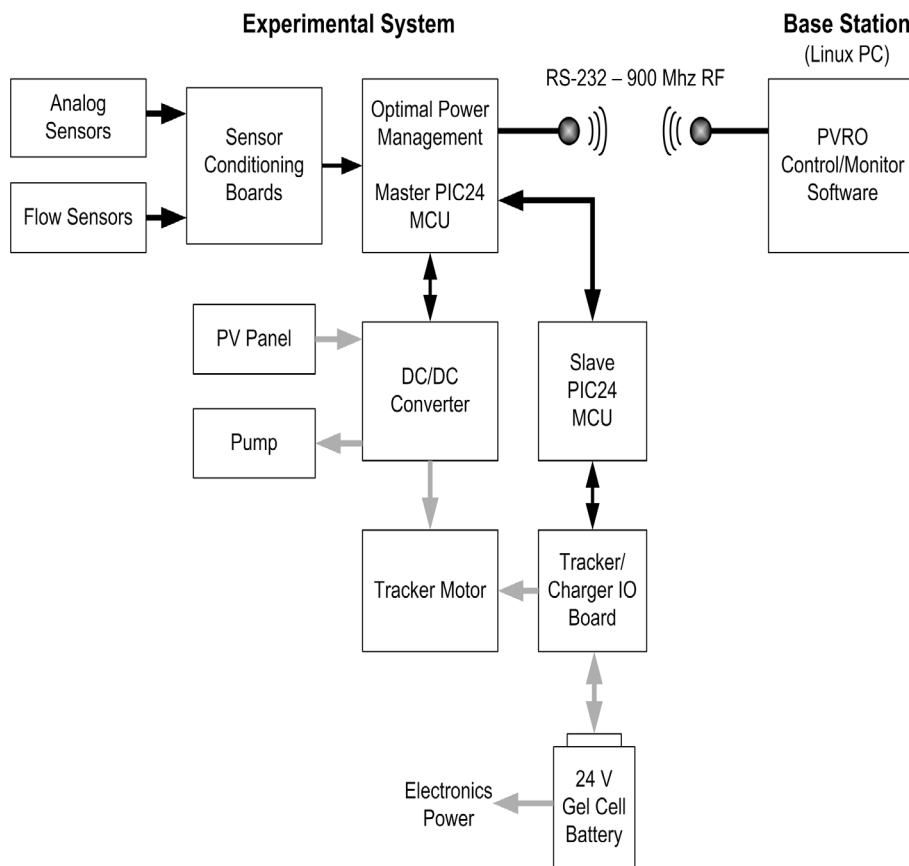


Fig. 9. Experimental system data acquisition, control and power architecture.

the solar panel tracker motors. The Master PIC24 also communicates with a base station PC running Linux over a wireless modem. The base station is used to record the acquired data and to display it in real time.

A model of the experimental system was developed using the framework outlined in Section 3 above. The system parameters for this model of the experimental system are shown in Table 3. These parameters were

Table 3
Experimental system model parameters

Component	Parameter	Value	
Sunpower 230W solar panel [23]	Solar cell area, A_c	1.489×10^{-3}	
	Light current constant, C_0	3.318 A/W	
	Light current temperature dependence constant, C_1	2.525×10^{-3} A/W-K	
	Normal operating cell temperature, NOCT	45°C	
	Number of solar cells connected in a string, n_{cell}	72	
	Number of strings connected in parallel, n_{string}	1	
	Solar cell series resistance, R_s	$1.911 \times 10^{-3} \Omega$	
	Solar cell shunt resistance, R_{sh}	1296 Ω	
	Shurflo 8050-243-169 pump & motor	Pump coefficient of viscous drag c_d	3.803×10^{-4} N-m/bar-L
		Pump friction coefficient, c_f	4.033 N-m/bar-L
Pump slip coefficient, c_s		3.361×10^{-10}	
Pump volumetric displacement per revolution, D		2.60×10^{-3} L/rev	
Motor friction related current, I_0		0.65 A	
Motor torque constant, K_T		2.252 A/N-m	
Motor speed constant, K_V		1.824 rev/V-s	
Motor resistance, R_m		0.1546 Ω	
Pump torque constant, T_c		0.05 Nm	
DOW Filmtec SW30-2540 reverse osmosis membrane [24]		Membrane water permeability, A	3.111×10^{-4} L/m ² -bar-s
	Membrane salt permeability, B	1.9481×10^{-5} L/m ² -s	
	Membrane area, S_E	2.8 m ²	
Other system parameters	Feed water salt concentration, C_f	35000 mg/L	
	Clark pump recovery ratio, R_1	0.090	

determined through manufacturer-supplied data and component characterization.

The experimental system has been tested under a variety of different weather conditions using a simple conventional maximum power point tracking control. Here, data from a partly day is used to validate the system models. The experimental system model outlined above was simulated for the mostly sunny day using the data collected for solar radiation (shown in Fig. 10), ambient

temperature, water salinity, and water temperature as inputs.

Fig. 11 shows the water production predicted by the model and the experimentally measured water production. The predicted and experimentally measured results agree well, with a difference of 5% between measured and predicted performance. As expected, the system produced approximately 300 L of clean water.

The overall experimental reverse osmosis system

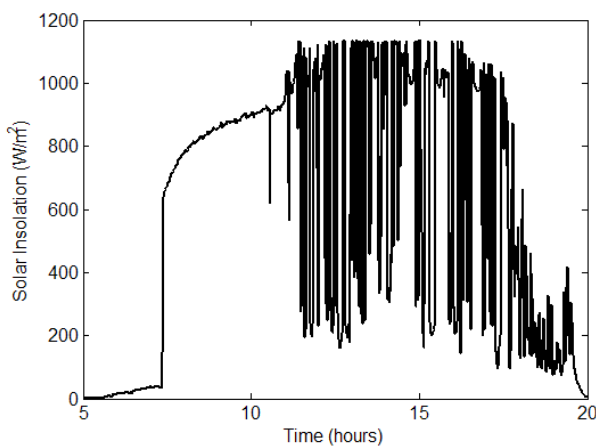


Fig. 10. Solar radiation incident on solar panel.

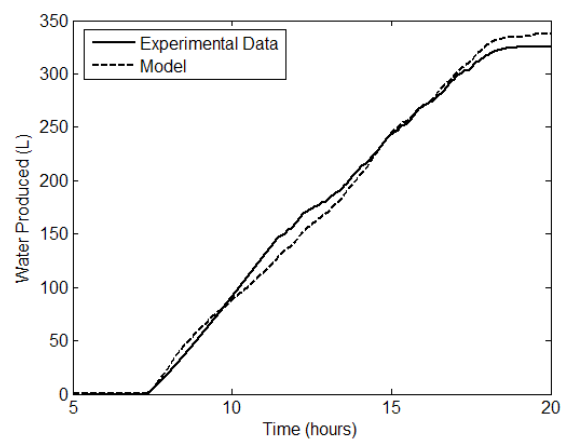


Fig. 11. Water produced over course of the day.

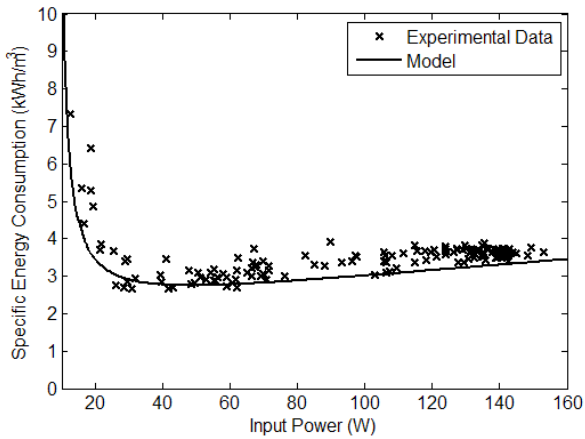


Fig. 12. Overall reverse osmosis system efficiency.

efficiency was also calculated and compared to the modeled results (see Fig. 12). The model agrees well with the experimental data. The overall specific energy consumption of the experimental system ranges between 4 kWh/m³ and 2.5 kWh/m³ when there is a reasonable input power available.

5. Conclusions

This paper has presented the motivation for the PVRO control research currently being conducted. A feasibility study was performed, which found that the geographic regions where PVRO is cost effective for small, remote communities can be increased by improving overall system efficiency, and that research in improved total system efficiency using smart control techniques is needed. Experimentally validated system models of small-scale PVRO systems have been developed for use for control algorithm design. Preliminary experimental results show good agreement with the models.

Acknowledgements

The authors would like to thank the King Fahd University of Petroleum and Minerals in Dhahran, Saudi Arabia, for funding the research reported in this paper through the Center for Clean Water and Clean Energy at MIT and KFUPM. The authors acknowledge efforts of KFUPM Team members in this joint collaborative research. The authors would also like to thank the Cyprus Institute for their fellowship support of Ms. Bilton.

Symbols

A — Reverse osmosis membrane water permeability, L/m²-bar-s
 A_c — Solar cell area, m²
 A_p — Area of the Clark pump piston, m²

A_r — Area of the Clark pump connecting rod, m²
 B — Reverse osmosis membrane salt permeability, L/m²-s
 C_b — Brine salt concentration, mg/L
 C_f — Feed water salt concentration, mg/L
 C_{fc} — Average concentration of the water on the concentrate side of the membrane, mg/L
 C_0 — Solar cell-specific light current constant, 1/V
 C_1 — Solar cell-specific light current temperature dependence constant, 1/V-K
 c_d — Pump coefficient of viscous drag, N-m/bar-L
 c_f — Pump geometry friction coefficient, N-m/bar-L
 c_s — Pump slip coefficient, Pa/bar
 D — Pump volumetric displacement per revolution, L/rev
 FF — Reverse osmosis membrane fouling factor
 G_{dir} — Direct solar radiation in plane normal to incoming rays, W/m²
 $G_{mod,dif}$ — Diffuse panel radiation, W/m²
 $G_{mod,ref}$ — Reflected panel radiation, W/m²
 $G_{mod,tot}$ — Total panel incident solar radiation, W/m²
 I_{cell} — Total solar cell current, A
 I_{D1} — Solar cell current losses due to recombination in bulk material, A
 I_{D2} — Solar cell current losses due to recombination in space charge region, A
 I_{module} — Solar module current, A
 I_{motor} — motor current, A
 I_{ph} — Solar cell light generated current, A
 I_{string} — Current produced by string solar cells, A
 I_0 — Motor friction related current, A
 K_T — Motor torque constant, A/N-m
 K_V — Motor speed constant, rev/V-s
 $NOCT$ — Normal solar cell operating temperature, K
 n — Pump speed, rev/s
 n_{cell} — Number of solar cells connected in a string
 n_{string} — Number of strings connected in parallel
 P_C — Pressure of brine entering the Clark pump, bar
 P_E — Pressure of brine exiting the Clark pump, bar
 P_F — Feed water pressure entering Clark pump, bar
 P_H — Pressure of the feed water entering the RO pressure vessel, bar
 P_L — Clark pump pressure losses, bar
 P_p — Permeate pressure, bar
 p_f — Membrane concentration polarization factor
 Q — Pump flow rate, L/s
 Q_C — Clark pump entering brine flow rate, L/s
 Q_E — Clark pump exiting brine flow rate, L/s
 Q_F — Medium pressure feed flow rate, L/s
 Q_L — Clark pump leakage flow rate, L/s
 Q_R — Flow loss due to pump inlet flow restriction, L/s
 Q_p — Permeate flow rate, L/s
 R_m — Motor resistance, Ω
 R_s — Solar cell series resistance, Ω
 R_{sh} — Solar cell shunt resistance, Ω

R_t	— Clark pump recovery ratio
S_E	— Reverse osmosis membrane surface area, m^2
T_{amb}	— Ambient temperature, K
T_c	— Pump torque constant, Nm
T_{cell}	— Cell temperature, K
TCF	— Membrane permeability temperature correction factor
V	— Solar cell operating voltage, V
V_m	— Motor internal back-EMF, V
V_{module}	— Solar module operating voltage, V
V_{motor}	— Motor voltage, V
V_{string}	— Voltage of string of solar cells, V

Greek

α	— Sun elevation angle, radians
β	— Solar module tilt angle, radians
$\Delta \bar{P}$	— Average pressure applied across the membrane, bar
ΔP_{fc}	— Pressure drop over membrane module, bar
Δp	— Pressure difference across the pump, bar
$\Delta \bar{\pi}$	— Average osmotic pressure across the membrane, bar
η_{mppt}	— Power electronics conversion efficiency
μ	— Dynamic viscosity of the water, bar-s
Ω	— Motor rotor speed, rev/s
π_b	— Brine osmotic pressure, bar
π_f	— Feed osmotic pressure, bar
π_p	— Permeate osmotic pressure, bar
ψ	— Solar module azimuth angle, radians
θ	— Sun azimuth angle, radians
τ	— Motor shaft torque, Nm

References

- [1] World Health Organization and UNICEF, Meeting the MDG drinking water and sanitation target, 2006, http://www.who.int/water_sanitation_health/monitoring/jmpfinal.pdf, accessed April 3, 2009.
- [2] United Nations, World Water Day 2007 Brochure – Coping With Water Scarcity, 2007, <http://www.unwater.org/wwd07/downloads/documents/wwd07brochure.pdf>, accessed on April 3, 2009.
- [3] United Nations World Water Assessment Programme, The 2nd United Nations World Water Development Report - Water: A Shared Responsibility, 2006, <http://unesdoc.unesco.org/images/0014/001454/145405E.pdf>, accessed December 18, 2009.
- [4] D. Harold and A. Neskakis, A small PV-driven reverse osmosis desalination plant on the island of Gran Canaria. *Desalination*, 137 (2001) 285–292.
- [5] Spectra Watermakers, SSW 3500 Datasheet, 2009, http://www.spectrawatermakers.com/landbased/products_ssw3500.php, accessed February 5, 2009.
- [6] A.M. Thomson, Reverse-osmosis desalination of seawater powered by photovoltaics without batteries. PhD thesis, Loughborough University, 2003.
- [7] S. Dallas, N. Sumiyoshi, J. Kirk, K. Matthew and N. Wilmot, Efficiency analysis of the Solarflow — An innovative solar-powered desalination unit for treating brackish water. *Renewable Energy*, 34(2) (2009) 397–400.
- [8] S. Cheah, Photovoltaic reverse osmosis desalination system, ITN Energy Systems, Inc., Report No. 104, Littleton, CO, 2004, <http://www.usbr.gov/pmts/water/publications/reportpdfs/report104.pdf>, accessed February 5, 2009.
- [9] A. Bilton, S. Dubowsky, R. Wiesman, A. Arif and S. Zubair, On the feasibility of community-scale photovoltaic-powered reverse osmosis desalination systems for remote locations, *Renewable Energy*, submitted.
- [10] Z. Al Suleimani and N.R. Nair, Desalination by solar powered reverse osmosis in a remote area of Sultanate of Oman. *Appl. Energy*, 64 (2000) 367–380.
- [11] E.H. Mohamed and G. Papadakis, Design, simulation and economic analysis of a stand-alone reverse osmosis desalination unit powered by wind turbines and photovoltaics, *Desalination*, 164 (2004) 87–97.
- [12] A.M. Helal, S.A. Al-Malek and E.S. Al-Katheeri, Economic feasibility of alternative designs of a PV-RO desalination unit for remote areas in the United Arab Emirates. *Desalination*, 221 (2008) 1–16.
- [13] H.M. Ettouney, H.T. El-Dessouky, R.S. Faibish and P.J. Gowin, Evaluating the economics of desalination. *Chem. Eng. Progr.*, 12 (2002) 32–38.
- [14] National Aeronautics and Space Administration, NASA Surface meteorology and solar energy: Global data sets, National Aeronautics and Space Administration, Atmospheric Science and Data Center, 2009, <http://eosweb.larc.nasa.gov/sse/>, accessed December 10, 2009.
- [15] National Oceanographic Data Center (US), Ocean Climate Laboratory, 2005 World ocean atlas. Washington, DC: US Dept. of Commerce, National Oceanic and Atmospheric Administration, 2005.
- [16] R. Wiser, P. Cappers, M. Bolinger and R. Margolis, Letting the sun shine on solar costs: An empirical investigation of photovoltaic cost trends in California. LBNL-59282, Berkeley, California, 2006.
- [17] United States Energy Information Administration, Annual US No. 2 diesel retail sales by all sellers, Decwmbler 1, 2009, <http://tonto.eia.doe.gov/dnav/pet/hist/d220600002m.htm>, accessed December 12, 2009.
- [18] F. Krieth and J.F. Kreider, Principles of Solar Engineering, Washington, Hemisphere Pub. Corp., 1978.
- [19] C. Rigollier, O. Bauer and L. Wald, On the clear sky model of the ESRA — European Solar Radiation Atlas — with respect to the Heliosat method, *Solar Energy*, 68(1) (2000) 33–48.
- [20] J.P. Charles, G. Bordure, A. Khoury and P. Mialhe, Consistency of the double exponential model with the physical mechanisms of conduction for a solar cell under illumination, *J. Phys. D: Appl. Phys.*, 18(11) (1985) 2261–2268.
- [21] FILMTEC Membranes System Design: System Performance Projection, vol. Form Number 609-02057-604, Dow Chemical Corporation, <http://www.dow.com>, accessed April 13, 2009.
- [22] ASTM, D4516-85 Standard Practice for Standardizing Reverse Osmosis Performance Data, 1985.
- [23] Sun Power Corp. 230 Watt Panel, S.P. Corp., ed., Sun Power Corp. Document #001-60680 Rev** February 2010.
- [24] FILMTEC Tape-Wrapped 2540 Elements for Commercial Applications, vol. Form No. 609-09030-0606 Dow Chemical Corporation, <http://www.dow.com>, Accessed April 10, 2010.